



PCCP

**Nuclear Quantum Effects on the Thermodynamic, Structural,
and Dynamical Properties of Water**

Journal:	<i>Physical Chemistry Chemical Physics</i>
Manuscript ID	CP-ART-08-2020-004325.R1
Article Type:	Paper
Date Submitted by the Author:	14-Feb-2021
Complete List of Authors:	Eltareb, Ali; Brooklyn College, Physics; CUNY The Graduate Center, Lopez, Gustavo; Lehman College of the City University of New York, Chemistry Giovambattista, Nicolas; CUNY, Brooklyn College

SCHOLARONE™
Manuscripts

Cite this: DOI: 00.0000/xxxxxxxxxx

Nuclear Quantum Effects on the Thermodynamic, Structural, and Dynamical Properties of Water[†]

Ali Eltareb,^{a,c} Gustavo E. Lopez,^{b,d} and Nicolas Giovambattista^{a,c,d}Received Date
Accepted Date

DOI: 00.0000/xxxxxxxxxx

We perform path-integral molecular dynamics (PIMD) simulations of H_2O and D_2O using the q-TIP4P/F model. Simulations are performed at $P = 1$ bar and over a wide range of temperatures that include the equilibrium ($T \geq 273$ K) and supercooled ($210 \leq T < 273$ K) liquid states of water. The density of both H_2O and D_2O calculated from PIMD simulations are in excellent agreement with experiments in the equilibrium and supercooled regimes. We also evaluate important thermodynamic response functions, specifically, the thermal expansion coefficient $\alpha_P(T)$, isothermal compressibility $\kappa_T(T)$, isobaric heat capacity $C_P(T)$, and static dielectric constant $\epsilon(T)$. While these properties are in excellent [$\alpha_P(T)$ and $\kappa_T(T)$] or semi-quantitative agreement [$C_P(T)$ and $\epsilon(T)$] with experiments in the equilibrium regime, they are increasingly underestimated upon further cooling. It follows that the inclusion of nuclear quantum effects in PIMD simulations of (q-TIP4P/F) water is not sufficient to reproduce the anomalous large fluctuations in density, entropy, and electric dipole moment characteristic of supercooled water. It has been hypothesized that water may exhibit a liquid-liquid critical point (LLCP) in the supercooled regime at $P > 1$ bar and that such a LLCP generates a maximum in $C_P(T)$ and $\kappa_T(T)$ at 1 bar. Consistent with this hypothesis and in particular, with experiments, we find a maximum in the $\kappa_T(T)$ of q-TIP4P/F light and heavy water at $T \approx 230 - 235$ K. No maximum in $C_P(T)$ could be detected down to $T \geq 210$ K. We also calculate the diffusion coefficient $D(T)$ of H_2O and D_2O using the ring-polymer molecular dynamics (RPMD) technique and find that computer simulations are in remarkable good agreement with experiments at all temperatures studied. The results from RPMD/PIMD simulations are also compared with the corresponding results obtained from classical MD simulations of q-TIP4P/F water where atoms are represented by single interacting sites. Surprisingly, we find minor differences in most of the properties studied, with $C_P(T)$, $D(T)$, and structural properties being the only (expected) exceptions.

1 Introduction

Water is one of the most important substances on Earth; it is the solvent of life as we know it^{1,2} and it plays a fundamental role in numerous scientific and engineering applications³. Yet, after centuries of being a target of scientific scrutiny, water's thermodynamic and dynamical properties remain puzzling, particularly, in the supercooled and glassy state⁴⁻¹⁰. One of the main open

questions in the field of water is whether there is a liquid-liquid critical point (LLCP) in its phase diagram at supercooled temperature^{4,5,11-13}. The so-called LLCP hypothesis for water was formulated in 1992, based on results from classical molecular dynamics simulations using the ST2 water model¹⁴. In this scenario, water at low temperatures exists in two different liquid states that are separated by a liquid-liquid phase transition (LLPT). In the P-T plane, the LLPT line ends at a LLCP, estimated to be located at $T \approx 220$ K and $P \approx 100$ MPa¹⁵⁻¹⁷; at low temperatures, the LLPT line extends into the glass state leading to two different glass states. The presence of two different glass states in water is consistent with experiments^{6,18-23} and computer simulations²⁴⁻³⁰. The LLCP hypothesis has been controversial from its early times and numerous studies have been published in favor (see, e.g., Refs. 11,12,25,29,31-36) and against it (see, e.g., Refs. 37-42). At present, it is fair to say that, from the computer simulations perspective, the evidence in favor of the existence of the LLCP is

^a Department of Physics, Brooklyn College of the City University of New York, Brooklyn, NY 11210, United States. E-mail: ali.eltareb@brooklyn.cuny.edu, ngiovambattista@brooklyn.cuny.edu

^b Department of Chemistry, Lehman College of the City University of New York, Bronx, NY 10468. E-mail: gustavo.lopez1@lehman.cuny.edu

^c Ph.D. Program in Physics, The Graduate Center of the City University of New York, New York, NY 10016

^d Ph.D. Program in Chemistry, The Graduate Center of the City University of New York, New York, NY 10016

[†] Electronic Supplementary Information (ESI) available: [details of any supplementary information available should be included here]. See DOI: 00.0000/00000000.

well-established. Popular models such as the ST2, TIP4P/2005, TIP4P/ice water models exhibit a LLCP^{14,31,43–51} while others, such as the mW and SPC/E models, do not^{52,53}. In this regard, we stress that the TIP4P/2005 and TIP4P/ice water models are among the best rigid classical models that reproduce the properties of water⁵⁴. Proving the existence of a LLCP in water has been challenging due to rapid crystallization at low temperatures. A recent experiment indicates that, indeed, water exhibits a LLPT²³ and strong support to the LLCP hypothesis for water can also be found in the recent experiments of Refs.^{11,12,55–57}.

While the postulated LLCP has not been observed in experiments due to rapid crystallization, the LLCP scenario predicts some anomalous signatures at temperatures that can be tested. Specifically, the existence of a LLCP in supercooled water at $P > 1$ bar requires that both $C_P(T)$ and $\kappa_T(T)$ exhibit a maxima at low pressures. This implies that upon cooling at 1 bar, both properties should increase and reach a maximum at a specific temperature, and then decrease upon further cooling. At present, experiments have confirmed that both $C_P(T)$ and $\kappa_T(T)$ increase upon cooling at low pressures, including 1 bar. A maximum in $\kappa_T(T)$ has been recently observed in two independent experiments performed at normal and negative pressures^{11,56}. A maximum in $C_P(T)$ has also been recently observed in experiments performed at normal pressure⁵⁸.

At present, most of the computational studies that find a LLCP in supercooled water are based on the ST2, TIP4P/2005 and TIP4P/ice models where molecules are treated as rigid bodies. These computational studies are based on classical computer simulations where fluctuations due to nuclear quantum effects (NQE) are omitted. In principle, this can be problematic since water is a light molecule and the delocalization of the H atoms due to NQE can occur at relatively high temperatures⁵⁹. Indeed, NQE are responsible for the well-known difference in the melting temperature of H_2O and D_2O ($\delta T \approx 4$ K) as well as in the corresponding temperature of maximum density ($\delta T \approx 7$ K) and glass transition temperature ($\delta T \approx 10$ K)⁶⁰. Interestingly, early experiments in the glassy/crystalline domain indicate that the location of the LLCP in D_2O is ≈ 10 K below the LLCP of H_2O (at a similar pressure)^{61,62}. Computer simulations of water-like models confirm that the inclusion of NQE can shift the location of the LLCP in the P-T phase diagram and shift the location of the associated $C_P(T)$ and $\kappa_T(T)$ maxima lines^{63,64}. The inclusions of NQE can also change the shape/slope of the coexistence LLPT line and supercritical C_P maxima line in the P-T plane⁶⁴.

In this work, we perform path-integral molecular dynamics (PIMD) simulations of water using the q-TIP4P/F water model⁶⁵, a realistic model for water explicitly parameterized for PIMD simulations. One of the aims of this work is (i) to test whether PIMD simulations using the q-TIP4P/F model are able to reproduce relevant thermodynamic properties of water (density $\rho(T)$), thermal expansion coefficient ($\alpha_P(T)$), $C_P(T)$, $\kappa_T(T)$, dielectric constant ($\epsilon(T)$) and dynamics (diffusion coefficient, $D(T)$) at $P = 1$ bar and supercooled conditions. This model has been validated against experiments in liquid water mostly at room temperature and based on a few properties (density, ϵ , C_P and D) but its thermodynamic behavior in the low-temperature regime

is mostly unexplored. As shown in Ref.⁶⁵ and in this work, the performance of the q-TIP4P/F model in PIMD simulations, relative to experiments, seems to be as good as the performance of (a) the TIP4P/2005 water model in classical MD simulations (one of the best rigid, classical model for water), (b) advanced water models such as the MB-pol model⁶⁶, and (c) water models obtained by combining density functional theory with machine learning techniques^{43,67} or PIMD simulations⁶⁸. We also (ii) test whether NQE, as introduced in PIMD simulations, can reproduce the differences in the target thermodynamic and dynamical properties upon isotope substitution (H_2O and D_2O) over a wide range of temperature. The most important goal of this work is (iii) to test whether the signatures of the LLCP hypothesis, i.e., maxima in $C_P(T)$ and $\kappa_T(T)$, can be reproduced in PIMD simulations of q-TIP4P/F water at 1 bar. As far as we know, the LLCP scenario has not been tested in the supercooled regime using computer simulations that include NQE, such as PIMD techniques.

This work is organized as follows. In Sec. II we present the computer simulation details. In Sec. III we discuss the results of our quantum (and classical) simulations for H_2O and D_2O using the q-TIP4P/F water model. A summary is included in Sec. IV.

2 Simulation Method

Our results are based on PIMD simulations of a system composed of $N = 512$ light/heavy water molecules in a cubic box with periodic boundary conditions at constant temperature and pressure. H_2O/D_2O molecules are represented using the q-TIP4P/F model⁶⁵. This water model is based on the popular TIP4P/2005 model for water, commonly used in classical computer simulations. The q-TIP4P/F water model is optimized to be used in path integral computer simulations and is able to reproduce remarkably well the properties of water at normal conditions, including water structure (OO, OH and HH radial distribution functions), thermodynamic properties (including the density and specific heat), dynamics (diffusion coefficient) and infra-red spectra⁶⁵. In the ice domain, the q-TIP4P/F reproduces successfully the heat capacity at temperatures from 50 K to 250 K^{69,70}.

All PIMD simulations are performed using the OpenMM (version 7.4.0) software package⁷¹ at $P = 1$ bar and for temperatures $T = 210, 220, 230, 240, 250, 260, 280, 300, 325, 350, 375$ K. This temperature range includes the equilibrium liquid state and extends into the supercooled liquid regime of q-TIP4P/F water since the melting temperature of q-TIP4P/F in quantum simulations is $T_M = 251$ K (the melting temperature of the classical version of the q-TIP4P/F model is 259 K)^{65,72}. A stochastic (local) path integral langevin equation (PILE) thermostat⁷³ is used to keep the temperature of the system constant while a Monte Carlo barostat is used to maintain the pressure at $P = 1$ bar⁷¹. In our PIMD simulations, O and H are represented by $n_b = 32$ beads which is not uncommon for PI computer simulations of water at approximately $T > 200$ K^{59,65,74}. Short-range (Lennard-Jones pair potential) interactions are calculated using a cutoff $r_c = 1.0$ nm; long range electrostatic interactions are computed using the PME (Particle Mesh Ewald) method with the same cutoff r_c .

At a given T, the system is equilibrated for a time interval t_{eq} ,

Table 1 Equilibration and production simulation times used for H_2O in PIMD and *classical* MD simulations.

H_2O (Quantum)			H_2O (Classical)		
T[K]	t_{eq} [ns]	t_{prod} [ns]	T[K]	t_{eq} [ns]	t_{prod} [ns]
210	20	30	200	1100	3000
220	4	8	210	200	800
230	2	8	220	25	100
240	1	4	230	10	10
250	1	4	240	10	10
260	1	3	250	10	10
280	0.5	2	260	10	10
300	0.5	2	280	2.5	2.5
325	0.5	2	300	2.5	2.5
350	0.5	2	325	2.5	2.5
375	0.5	2	350	2.5	2.5
			375	2.5	2.5

Table 2 Equilibration and production simulation times used for D_2O in PIMD and *classical* MD simulations.

D_2O (Quantum)			D_2O (Classical)		
T[K]	t_{eq} [ns]	t_{prod} [ns]	T[K]	t_{eq} [ns]	t_{prod} [ns]
210	50	50	210	100	250
220	8	16	220	20	100
230	2	8	230	20	30
240	1	4	240	20	20
250	1	4	250	20	20
260	1	3	260	10	10
280	0.5	2	280	5	5
300	0.5	2	300	5	5
325	0.5	2	325	5	5
350	0.5	2	350	5	5
375	0.5	2	375	5	5

followed by a production run of time length t_{prod} . The values of t_{eq} and t_{prod} vary with temperature and are given in Table I and II, for the case of H_2O and D_2O , respectively; the simulation time step is $dt = 0.25$ fs. To confirm that the system reaches equilibrium, we monitor the mean-square displacement (MSD) of the system and extend the PIMD simulations to satisfy that (i) $t_{eq}, t_{prod} > \tau$, where τ is the time it takes for the MSD of the water molecules to reach 1 nm^2 . This roughly indicates that molecules diffuse over ≈ 0.3 nm, i.e., approximately the OO distance between neighboring water oxygens. In addition, we confirm that (ii) the system obeys the Einstein-Smoluchowski result, $MSD(t) \propto t$, in the diffusive regime. Conditions (i) and (ii) are satisfied in all our classical MD and PIMD simulations; see SM. Equilibrium simulations are run independently at $T \geq 260$ K while, at $T < 260$ K, simulations are run sequentially, e.g., the equilibrium run at $T = 240$ K starts from the last configuration obtained at $T = 250$ K. The thermostat collision frequency γ used during the equilibration and production runs is set to $\gamma = 0.001 \text{ ps}^{-1}$; we confirm that this value of γ does not affect the dynamics of the system (see SM).

PIMD simulations can be very sensitive to technical parameters such as the simulation time step and the number of beads per ring-polymer considered⁷⁵. In order to test the robustness of our results to variations of dt and n_b , we also perform additional PIMD simulations using $dt = 0.1, 0.25, 0.50$ fs and $n_b = 32, 72, 128$ (see

SM). Briefly, we find that water structure (e.g., radial distribution functions and local tetrahedral order) and diffusion coefficients are independent of dt , n_b , and γ . While some thermodynamic properties, such as density, are also robust to variations in these parameters, other properties such as the enthalpy of the system can vary with the time step and number of beads used. As we show below, such a sensitivity in the enthalpy can result in large variations in the isobaric heat capacity (see SM). Classical MD simulations of q-TIP4P/F water are also performed for comparison; this is done by collapsing the ring polymer to a single bead (i.e., by setting $n_b = 1$). For the classical simulations, a time step $dt = 0.50$ fs is used and the collision frequency is also set to $\gamma = 0.001 \text{ ps}^{-1}$.

3 Results

Our results are organized as follows. In Sec. 3.1, we discuss the thermodynamic properties of light/heavy water. Sec. 3.2 focuses on the diffusion coefficient of light/heavy water while structural properties are discussed in Sec. 3.3.

3.1 Thermodynamics

3.1.1 Liquid Density at normal pressure

The densities of H_2O and D_2O at $P = 1$ bar are shown in Fig. 1 for temperatures ranging from $T = 210$ K to 375 K. For comparison, included are densities reported from independent computational studies. The densities obtained from our PIMD simulations for H_2O (blue circles in Fig. 1a) are in good agreement with the densities obtained from PIMD simulations of q-TIP4P/F water reported by Habershon et al. (magenta squares)⁶⁵ and Herrero and Ramirez (red up-triangles)⁶⁹. Similarly, our densities for D_2O (red circles in Fig. 1b) are in good agreement with the value reported by Habershon et al. (black square) at $T = 298 \text{ K}$ ⁶⁵.

Experimental densities for H_2O and D_2O are also included in Fig. 1. Overall, the densities of light and heavy q-TIP4P/F water are remarkably close to the corresponding experimental densities over the equilibrium and accessible supercooled liquid regimes, at approximately $T \geq 240 - 250$ K (crystallization becomes very difficult to overcome in experiments at lower temperatures and data is not available in the literature). The densities of q-TIP4P/F light and heavy water are larger than the experimental data by only $\approx 0.005 - 0.01 \text{ g/cm}^3$ (representing a relative error of 0.5 - 1.0%).

H_2O and D_2O are anomalous liquids with a well-known density maxima at $T_{M,H_2O} = 277$ K and $T_{M,D_2O} = 284$ K (see Fig. 1). The corresponding values for light/heavy q-TIP4P/F water are $T_{M,H_2O} = 280$ K and $T_{M,D_2O} = 282$ K. These values are reasonable close to the corresponding experimental temperatures. However, the temperature difference in the location of the density maxima of H_2O and D_2O is $\Delta T_M = T_{M,D_2O} - T_{M,H_2O} \approx 7$ K in experiments while in our PIMD simulations, $\Delta T_M \approx 2$ K.

In order to compare the differences between PIMD simulations and classical MD simulations, we also include in Fig. 1a the densities of TIP4P/2005 water (obtained from classical simulations; green squares) as well as the densities of the classical q-TIP4P/F model for H_2O (obtained by setting $n_b = 1$). We note that these

classical models consist of four interacting sites. However, while the TIP4P/2005 water model is rigid, the classical version of the q-TIP4P/F model is flexible. As shown in Fig. 1a, the differences in density between the classical and quantum q-TIP4P/F water models (black and blue circles) are negligible (and overlap within error bars). These densities are marginally larger than the densities of the (parent) TIP4P/2005 water (green squares). Similarly, as shown in Fig. 1b, the densities between the classical and quantum q-TIP4P/F model for D_2O are practically identical within error bars. It follows that, at least for the densities of liquid water, the classical flexible q-TIP4P/F water model can reproduce the experimental data of H_2O and D_2O relatively well for $T \geq 240$ K. The similarities between the properties of the classical ($n_b = 1$) and quantum ($n_b \geq 32$) q-TIP4P/F light water have been noticed in the past⁶⁵ and have been used as a motivation to study the phase diagram of ice using the classical (as opposite to quantum) q-TIP4P/F model⁷². It has been noticed that the similarities between the classical and PIMD version of the q-TIP4P/F models are due to the competition between intramolecular zero point fluctuations in the OH bond length, which weakens the strength of the hydrogen bonds, and fluctuations in the molecular dipole moment, which strengthens intermolecular interactions. These effects nearly cancel out in PIMD simulations of the q-TIP4P/F water, leading to a small NQE in this model^{65,68,76}. Thermodynamic properties of the classical and quantum q-TIP4P/F water are also similar in the supercooled regime as well as for the case of D_2O (see next sections).

3.1.2 Thermal expansion coefficient

Next, we discuss briefly the thermal expansion coefficient of water,

$$\alpha_p(T) = \frac{1}{V} \left(\frac{\partial V}{\partial T} \right)_p \quad (1)$$

which is a relevant thermodynamic response function used to characterize liquids. Fig. 2 shows $\alpha_p(T)$ at $P = 1$ bar for H_2O and D_2O from PIMD simulations based on the q-TIP4P/F model. For comparison we have also included computer simulation results based on the corresponding classical version of the q-TIP4P/F water model. The values of $\alpha_p(T)$ (dashed lines) are obtained by definition, using Eq. 1. The inset of Fig. 2 shows the volume of the systems studied as function of T; the dashed-lines are third-order polynomials fit of the data which is then used in Eq. 1. The results shown in Fig. 2 for the classical and quantum q-TIP4P/F water are practically indistinguishable (blue and black lines) and overlap with the results reported for TIP4P/2005 water in Ref.⁵⁴ (green squares). Similarly, the same values of $\alpha_p(T)$ follow from the classical/quantum q-TIP4P/F heavy water (green and red lines). The experimental values of $\alpha_p(T)$ for supercooled H_2O and D_2O are also included in Fig. 2 (blue and black triangles)⁷⁹. It follows that the q-TIP4P/F model is able to reproduce the experimental $\alpha_p(T)$ down to $T = 250 - 260$ K. Below $T = 260$ K, in the supercooled regime water, the classical/quantum q-TIP4P/F models overestimate $\alpha_p(T)$ (by up to 50%).

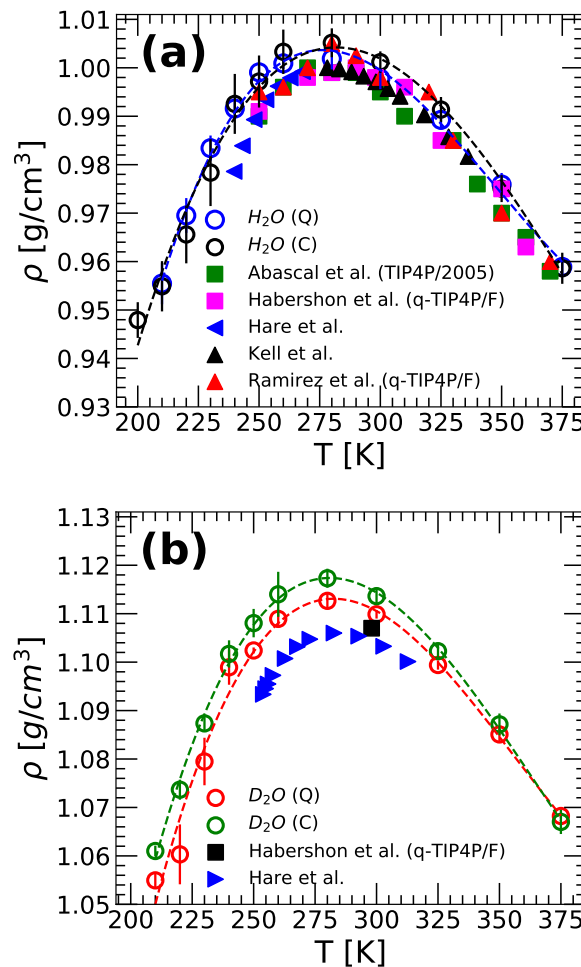


Fig. 1 (a) Density of H_2O as a function of temperature ($P = 1$ bar). Results from our PIMD simulations using the q-TIP4P/F water model are indicated by blue circles. These densities are in agreement with the densities obtained by Habershon et al.⁶⁵ (magenta squares) and Herrero and Ramirez⁶⁹ (red up-triangles) from PIMD simulations using the same water model. For comparison, we also include the water densities obtained from classical MD simulations using the q-TIP4P/F (flexible) water model ($n_b = 1$, this work; black circles) and the TIP4P/2005 (rigid) water model⁵⁴ (green squares). Experimental data in the equilibrium ($T > 273$ K) and supercooled regimes are taken from Ref.⁷⁷ (black up-triangles) and⁷⁸ (blue left-triangles). (b) Density of D_2O as a function of temperature ($P = 1$ bar) obtained from PIMD (red circles, this work; black square, Ref.⁶⁵) and classical MD simulations (green circles). Experimental densities in the equilibrium and supercooled regimes are from Ref.⁷⁹ (blue right-triangles). Dashed-lines are guides to the eye and are obtained by interpolating the densities of H_2O and D_2O using a third order polynomial. Error bars are the standard deviation of the densities obtained by using block-averaging.

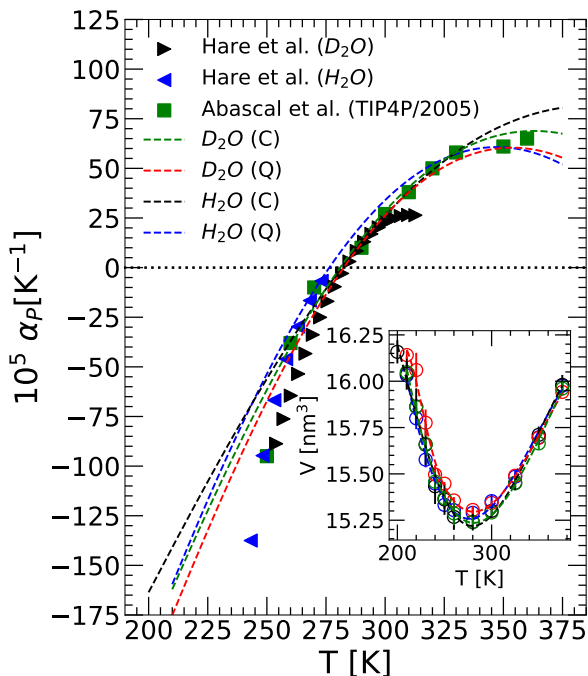


Fig. 2 Thermal expansion coefficient $\alpha_p(T)$ as a function of temperature at $P = 1$ bar. Results from PIMD simulations obtained using the q-TIP4P/F model for H_2O and D_2O are indicated by blue and red lines, respectively. Also included are the $\alpha_p(T)$ for H_2O and D_2O obtained from classical MD simulations using the q-TIP4P/F model (black and green lines, this work) and TIP4P/2005 (green squares, Ref. ⁵⁴). Experimental values of H_2O and D_2O in the equilibrium and supercooled regime are indicated by blue left-triangles and black right-triangles⁷⁹. $\alpha_p(T)$ is calculated from the volume of the system as function of temperature (inset). The volumes are fitted to a third order polynomial and then analytically differentiated (see Eq. 1).

3.1.3 Isothermal Compressibility

The isothermal compressibility

$$\kappa_T(T) = -\frac{1}{V} \left(\frac{\partial V}{\partial P} \right)_T \quad (2)$$

can be calculated from the volume fluctuations of the system⁸⁰,

$$\kappa_T(T) = \frac{\langle V^2 \rangle - \langle V \rangle^2}{k_B T \langle V \rangle} \quad (3)$$

where $\langle \dots \rangle$ indicates average over configurations and k_B is the Boltzmann's constant. In this work, we calculate $\kappa_T(T)$ (at $P = 1$ bar) using Eq. 3. We confirm that similar results are obtained by using Eq. 2.

Fig. 3a and 3b show, respectively, $\kappa_T(T)$ for H_2O and D_2O . The distinction between the classical and PIMD simulations are, again, negligible within error bars ($T \geq 210$ K); error bars shown in Fig. 3 are calculated using block-averaging to obtain $\kappa_T(T)$ and represent the corresponding standard deviation.

The isothermal compressibilities of q-TIP4P/F water (blue and black circles) practically overlap with the experimental data at approximately $T > 270$ K, corresponding to equilibrium water. In the supercooled regime, however, deviations between the simulation and experimental results become relevant and more pronounced upon supercooling. This is the typical behavior observed in classical water models, such as in the case of TIP4P/2005 water (green squares). It is apparent that introducing nuclear quantum effects via PIMD simulations is not sufficient to generate the density fluctuations occurring in real supercooled water. This indicates that the fluctuations in the hydrogen-bond network of q-TIP4P/F water need to be, somehow, enhanced at low-temperatures.

An important point of Fig. 3 is the presence of a minimum in the isothermal compressibility of classical/quantum H_2O and D_2O which are also found in experiments. In the case of PIMD and classical MD simulations, a clear maximum can also be observed in H_2O and D_2O . The minimum and maximum in κ_T are two well-known anomalous properties of light/heavy water that play a fundamental role in elucidating the phase behavior of supercooled and glassy water (see e.g., Refs. ^{5,27,48,81}). Specifically, their presence is a strong indication that water may have a liquid-liquid critical point at low-temperatures and positive pressures^{5,6,12,14,56}. In this regard, it is particularly relevant to find that including nuclear quantum effects does not eliminate the extrema in the isothermal compressibility. We note that in the case of H_2O , the isothermal compressibility reaches a minimum for the quantum and classical simulations at a temperature around $T_m^K \approx 310$ K, which is close to the experimental value $T_m^K = 319$ K⁴. The maximum in $\kappa_T(T)$ from PIMD and classical simulations occurs at $T_M^K \approx 230$ K, which is very close to the experimental $T_M^K = 228$ K reported by Kim et al.¹¹. Similarly, in the case of D_2O , we find that $T_m^K \approx 315$ K and $T_M^K \approx 235$ K, close to the experimental values, $T_m^K \approx 322$ K and $T_M^K \approx 233$ K¹¹.

3.1.4 Enthalpy and Isobaric Heat Capacity

Fig. 4 shows the enthalpy $H(T)$ and isobaric heat capacity

$$C_P(T) = (\partial H / \partial T)_P \quad (4)$$

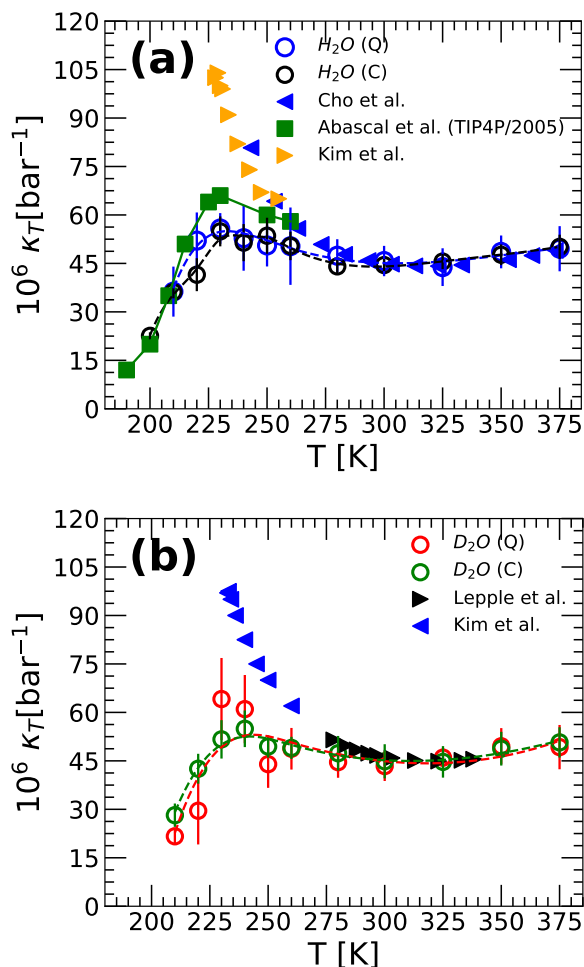


Fig. 3 (a) Isothermal compressibility $\kappa_T(T)$ as a function of temperature at $P = 1 \text{ bar}$. Results from PIMD simulations using the q-TIP4P/F model for H_2O are indicated by blue circles. Compressibilities obtained from classical MD simulations using the q-TIP4P/F and TIP4P/2005 water models are indicated by black circles (this work) and green squares (from Ref.⁸²). Values for $\kappa_T(T)$ are calculated by evaluating the volume fluctuations in the system. Experimental data for the $\kappa_T(T)$ of water is also included (blue left-triangles from Ref.⁴, orange right-triangles from Ref.¹¹). The $\kappa_T(T)$ obtained from simulations and experiments (orange triangles) exhibit an anomalous maximum at $T \approx 230 \text{ K}$, consistent with the possibility of a LLCP at low temperatures. (b) Results from PIMD and classical MD simulations using the q-TIP4P/F model for D_2O (red and green circles, respectively). Experimental data for the $\kappa_T(T)$ of heavy water is also included (blue left-triangles; from Ref.¹¹ and black right-triangles from Ref.⁸³). The experimental data from Kim et al. (left-blue triangles) also exhibits a maximum at $T = 229 \text{ K}$.

for H_2O and D_2O obtained from our PIMD simulations using the q-TIP4P/F model. Since the energy of the system may be sensitive to n_b , in this section, we also include results obtained with $n_b = 72$ (results with $n_b = 128$ are included in the SM). Also included are results from MD simulations based on the classical version of the q-TIP4P/F model for H_2O and D_2O as well as the corresponding experimental data. $C_p(T)$ is calculated using Eq. (4) where $H(T)$ is obtained directly from the PIMD simulations performed at different temperatures, and then fitted by using a third-order polynomial. It follows from Fig. 4 that nuclear quantum effects are relevant for the calculations of both $H(T)$ and $C_p(T)$. As shown in Fig. 4b and 4c, the classical values of $C_p(T)$ are much larger from those obtained using PIMD simulations for both light and heavy water, and from the experimental data. The failure of classical models to reproduce the experimental $C_p(T)$ is well-known⁸⁴ and it is expected since the estimators for the energy (and enthalpy) of the ring-polymer system and the associated quantum liquid are different⁸⁵. For example, the C_p values for the TIP4P/2005 water model are larger than the experimental values by 10 J/mol/K (green squares)⁵⁴. In the case of the classical q-TIP4P/F model for light and heavy water, the values of $C_p(T)$ are further off from the experimental values by $20 - 50 \text{ J/mol/K}$ for $T > 250 \text{ K}$.

The q-TIP4P/F model is able to reproduce relatively well the experimental $C_p(T)$ for both H_2O and D_2O once nuclear quantum effects are included in PIMD simulations. Our values of $C_p(T)$ for H_2O at $T = 273 \text{ K}$ using $n_b = 32$ (blue line) are slightly larger than the corresponding value reported by Herrero et al. (red triangle in Fig. 4b⁶⁹). However, $C_p(T)$ decreases considerably if one uses $n_b = 72$. Evidently, the values of $C_p(T)$ are very sensitive to the parameters employed in the PIMD simulations. As shown in the SM, variations in the simulation time step ($dt = 0.1 - 0.5 \text{ fs}$) and number of beads per polymer ($n_b = 32 - 128$) can lead to changes in $C_p(T)$ of $5 - 50 \text{ J/mol/K}$ (yet, PIMD simulations should converge to the correct values of C_p for sufficiently large n_b and small dt). In this regard, it would be desirable to employ PIMC simulations, instead of PIMD simulations, to calculate C_p since, in PIMC simulations, parameters such as dt and γ are not needed. In this context, we note that PIMC simulations employing the (rigid) TIP4PQ/2005 water model show that the values of C_p for this model (blue down-triangle in Fig. 4b) are in extremely good agreement with experiments, at least at $T \geq 260 \text{ K}$ ⁸⁴.

Regardless of the water model employed (rigid/flexible), neither classical MD nor PIMD simulations (including NQE) are able to reproduce the sharp increase of $C_p(T)$ in the supercooled domain at $T < 260 \text{ K}$. It is probable that other sources of entropy fluctuations, beyond the quantum fluctuations already considered in PIMD simulations, are needed in order to reproduce the apparent divergency in the experimental $C_p(T)$ (at $T < 240 \text{ K}$). This is consistent with Fig. 3 where the compressibility of q-TIP4P/F water is shown to be smaller than the compressibility of real water. In other words, our simulations show smaller density and entropy fluctuations than those occurring in real water (at low temperatures). Similarly, the recent experimental values of C_p reported by Pathak et al.⁵⁸ for the case of H_2O show a maximum at $T \approx 229 \text{ K}$. However, a maximum in C_p is not detectable in our MD and PIMD simulations at $T \geq 210 \text{ K}$.

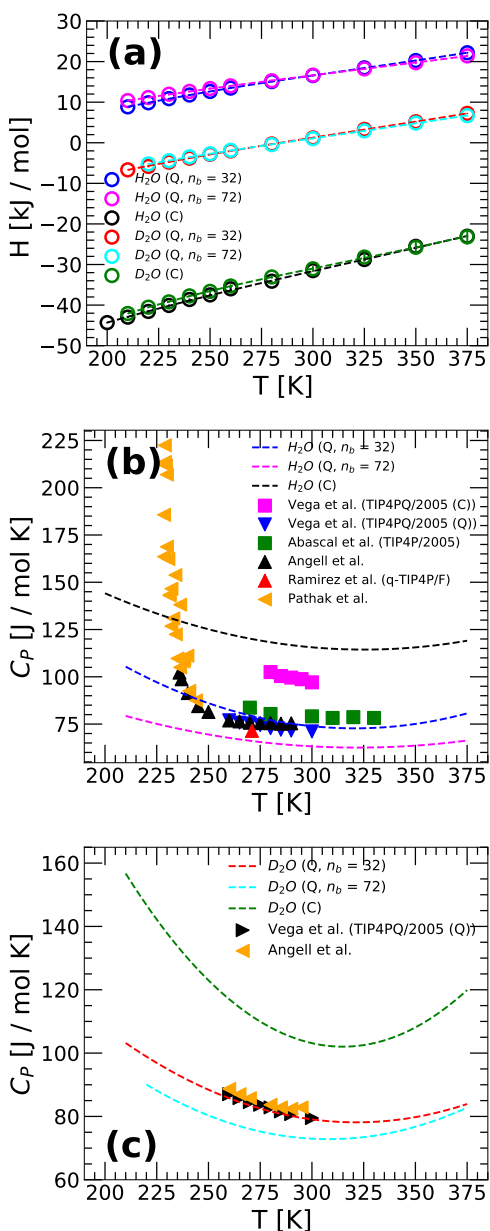


Fig. 4 (a) Enthalpy as a function of temperature for H_2O and D_2O at $P = 1$ bar. Blue and magenta circles are the enthalpies of H_2O obtained from PIMD simulations using $n_b = 32$ and 72 beads for all temperatures, respectively (q-TIP4P/F model). The enthalpies of D_2O are shown by red and cyan circles for $n_b = 32$ and 72 beads, respectively (q-TIP4P/F model). Black and green circles are results from classical MD simulations using the q-TIP4P/F model. Lines are obtained using third-order polynomial fits. (b) Heat capacity of H_2O as a function of temperature $C_p(T)$ calculated by differentiation from (a) using Eq. 4 (black, magenta, and blue lines). For comparison, we also include the $C_p(T)$ obtained from PIMD simulations of q-TIP4P/F water from Ref.⁶⁹ (red up-triangles) and TIP4PQ/2005 water from Ref.⁸⁴ (blue down-triangles). Green squares indicate the $C_p(T)$ of water from classical MD simulations using the TIP4P/2005 model⁵⁴. Experimental values of $C_p(T)$ for H_2O are also shown for comparison (black up-triangles, left-orange triangles; from Refs.^{58,86}, respectively). (c) Heat capacity of D_2O as a function of temperature calculated from (a) (green and red lines). For comparison, we also include the $C_p(T)$ obtained from PIMD simulations of TIP4PQ/2005 water in Ref.⁸⁴ (black right-triangles). Experimental values of $C_p(T)$ for heavy water from Ref.⁸⁶ (orange left-triangles).

3.1.5 Dielectric Constant

The static dielectric constant $\epsilon(T)$ is shown in Fig. 5 and is calculated from the fluctuations in the total electric dipole moment of the system, \vec{M} ,

$$\epsilon(T) = 1 + \frac{4\pi}{3\langle V \rangle k_B T \epsilon_0} (\langle \vec{M}^2 \rangle - \langle \vec{M} \rangle^2) \quad (5)$$

The error bars in Fig. 5 are calculated using block-averaging to obtain $\epsilon(T)$ and the corresponding standard deviation. The relatively large error bars are not surprising since the dielectric constant usually exhibits large fluctuations.

Figs. 5a and 5b show, respectively, $\epsilon(T)$ for H_2O and D_2O calculated from PIMD simulations using the q-TIP4P/F model. The $\epsilon(T)$ of H_2O and D_2O as obtained from classical MD simulations (q-TIP4P/F model) and from experiments are also included. In both H_2O and D_2O , the static dielectric constant of (classical and quantum) q-TIP4P/F water is shown to be in qualitative agreement with the experimental results, i.e., the dielectric constant increases as the temperature decreases. We note that the experimental results from Angell *et al.*⁸⁷ show that the dielectric constant seems to diverge at $T_s \approx 228$ K. Instead, our computer simulations from PIMD and classical MD predict that the dielectric constant should have a maximum, avoiding any divergency. It follows that the situation regarding $\epsilon(T)$, may be analogous to the case of $\kappa_T(T)$ where early works suggest an apparent divergency at $T_s \approx 228$ K⁸⁸ but more recent works indicate that, instead, $\kappa_T(T)$ exhibits a maximum at lower temperatures¹¹. As for the case of the compressibility maximum in water, a maximum in $\epsilon(T)$, which indicates a maximum in the fluctuations of the dipolar moment of water, could also be explained by the LLCP hypothesis scenario.

Interestingly, the values of $\epsilon(T)$ obtained from simulations are increasingly underestimated with increasing supercooling. As for the case of density fluctuations (κ_T) and entropy fluctuations (C_p), we find that dielectric dipole moment fluctuations (ϵ) cannot be reproduced by our PIMD simulations. This, again, suggests that the model employed and/or the inclusion of NQE in path integral simulations is, somehow, missing sources of fluctuations in the hydrogen-bonded network of water.

3.2 Dynamics

Next, we focus on the diffusivity of light and heavy water. Our results are based on the ring-polymer molecular dynamics (RPMD) methodology⁹¹. The RPMD approach to quantum dynamics uses the classical evolution of the ring-polymers in constant (N, V, E) PIMD simulations to calculate, approximately, the Kubo transformed correlation functions of the quantum system. In the RPMD approximation, the Kubo-transformed velocity autocorrelation function is given as⁹²

$$\tilde{c}_{\vec{v},\vec{v}} \approx \langle \vec{v}(0) \cdot \vec{v}(t) \rangle = \frac{1}{\Delta} \sum_{i=1}^{\Delta} \vec{v}(i) \cdot \vec{v}(i+t) \quad (6)$$

where $\vec{v}(i)$ is the bead-averaged velocity of the ring polymer and Δ is the total length of the RPMD trajectory. The self-diffusion

coefficient $D(T)$ can be obtained from⁶⁵

$$D = \frac{1}{3} \int_0^\infty \tilde{c}_{\vec{v},\vec{v}}(t) dt \quad (7)$$

Alternatively, it has been suggested⁹³ that the diffusion coefficient of the quantum liquid can be obtained from the mean-square displacement of the ring-polymer centroids, i.e.,

$$\lim_{t \rightarrow \infty} \frac{d}{dt} \langle |\vec{r}_i(t) - \vec{r}_i(0)|^2 \rangle = 6D \quad (8)$$

where $\vec{r}_i(t)$ is the position of the ring-polymer centroid associate to the O atom of molecule i at time t . It follows from Eq. 8 that

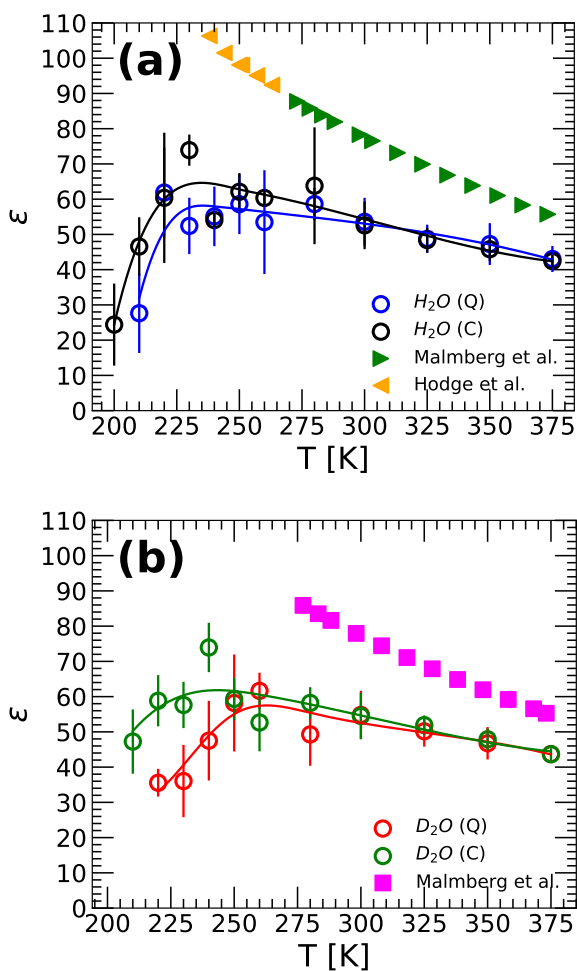


Fig. 5 (a) Dielectric constant of H_2O as a function of temperature at $P = 1$ bar. Blue and black circles are, respectively, results obtained from PIMD and MD simulations using the q-TIP4P/F model. Green and orange triangles are experimental values of the dielectric constant of water from Refs.^{87,89}, respectively. As for the case of $\kappa_T(T)$, an anomalous maximum in the dielectric constant in q-TIP4P/F water develops at low temperatures, consistent with the possibility of a LLCP in the deep supercooled regime. (b) The red circles are results obtained from PIMD simulations using the q-TIP4P/F model for the case of D_2O ; green circles are results from classical MD simulations using the same model. Experimental values for D_2O are taken from Ref.⁹⁰ (magenta squares).

one can evaluate $D(T)$ from the slope of the mean-square displacement of the molecules at long times in the so-called diffusive regime (see, e.g., Ref.⁹³).

In this work, the diffusion coefficient D is calculated from Eq. 8. However, instead of working in the NVE ensemble, we keep the local PILE thermostat on, alike thermostated RPMD (T-RPMD)⁹⁴. Yet, our method is not strictly T-RPMD. In T-RPMD using the local PILE thermostat, one should set the friction coefficient of the zero-frequency mode to zero ($\gamma = 0$)⁹⁴, while in our case, $\gamma = 0.001 \text{ ps}^{-1}$. Nonetheless, as shown in Fig. S6 of the SM, our results are independent of γ and hence, the thermostat has no effect on the dynamics. In the SM (Fig. S8), we show that the values of $D(T)$ obtained from Eq. 8 are identical (within error bars) to the values obtained using the NVE ensemble and Eq. 7.

The values of $D(T)$ for H_2O and D_2O are shown in Fig. 6. Included are results for the classical MD and PIMD simulations using the q-TIP4P/F model, available data from independent works (q-TIP4P/F model) as well as experimental data. Our results at $T = 300 \text{ K}$ for H_2O and D_2O are consistent with the values of D reported by Habershon *et al.*⁶⁵, obtained by using the RPMD technique and Eq. 7. Self-diffusion coefficients can be sensitive to the finite size of the system⁹⁵. The values of $D(T)$ shown in Fig. 6 do not include finite size effects. The corrections due to the system finite size are estimated following the procedure of Ref.⁹⁵ and are found to be minor ($< 10 - 15 \%$).

The results from computer simulations underestimate the experimental diffusivities of H_2O at approximately $T > 320 \text{ K}$ (Fig. 6a). For example, at $T \approx 373 \text{ K}$, the classical and quantum diffusivities for q-TIP4P/F water deviate by $\approx 0.15 - 0.20 \text{ \AA}^2/\text{ps}$ from the experimental value (a relative error of $\approx 19 - 25 \%$). At low temperatures, $T < 320 \text{ K}$, diffusivities in all models decrease and apparently converge to the experimental values of D , see Fig. 6a and 6b. To compare the experimental and computer simulations diffusivities at low temperature, we plot $D(T)$ as function of $1/T$ in Fig. 7. Experiments⁹⁹ show that water's diffusivity at $T \geq 240 \text{ K}$ is consistent with the prediction from mode coupling theory (MCT)¹⁰⁰, i.e.,

$$D = D_0(T - T_{MCT})^{\gamma_0} \quad (9)$$

where $\gamma_0 = 2.2$, $T_{MCT} = 221 \text{ K}$, and $D_0 = 1.43 \cdot 10^{-13} \text{ m}^2/\text{s}$. The solid lines in Fig. 7 are the fit of the $D(T)$ obtained from our classical MD and PIMD simulations of q-TIP4P/F water. It follows that MCT applies to classical and quantum q-TIP4P/F water at $T \geq 220 \text{ K}$. The corresponding fitting parameters are ($T_{MCT} = 200 \text{ K}$, $\gamma_0 = 2.27$) for the PIMD simulations and ($T_{MCT} = 209 \text{ K}$, $\gamma_0 = 2.25$) for the classical MD simulations. These values of γ_0 are remarkably close to the corresponding experimental value while the values for T_{MCT} are somewhat smaller than the corresponding experimental value.

Fig. 7 indicates that the diffusion coefficient of q-TIP4P/F water obtained from classical MD is always smaller than the corresponding values obtained from PIMD simulations. In other words, NQE enhance the mobility of water molecules. While this is expected, previous studies disagree on the quantitative effects that NQE have on water's diffusion coefficient. Specifically, early com-

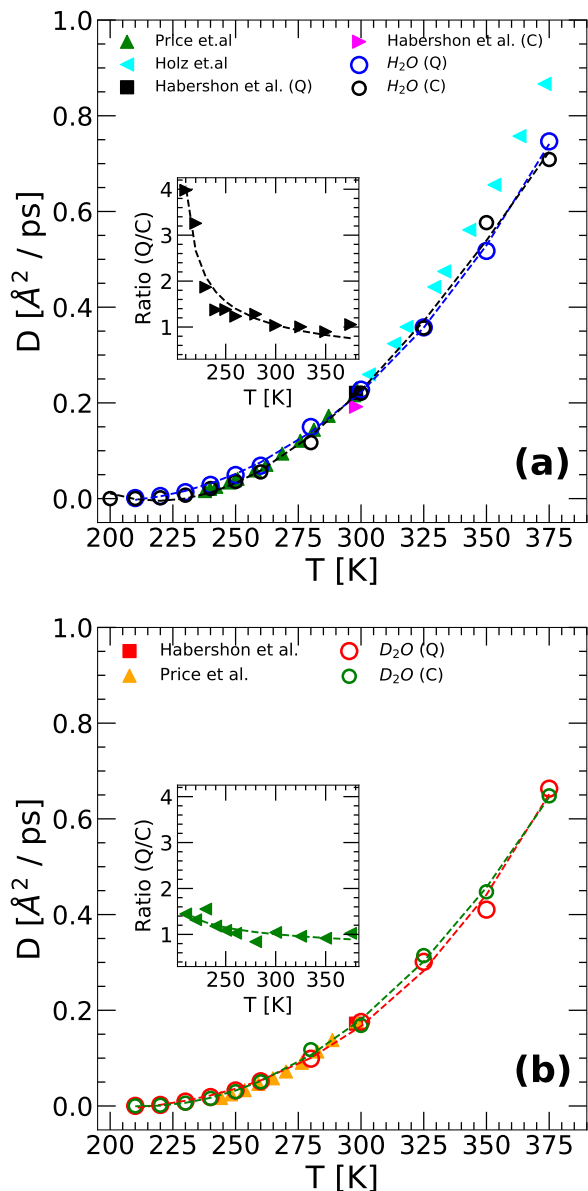


Fig. 6 (a) Diffusion coefficient of H_2O as a function of temperature ($P = 1$ bar) from PIMD simulations using the q-TIP4P/F model (blue circles); black circles represent the diffusion coefficient of q-TIP4P/F water from classical MD simulations ($n_b = 1$). The diffusion coefficient of q-TIP4P/F water at $T = 300$ K from PIMD simulations (black square) and classical MD simulations (magenta right triangle) reported in Ref. ⁶⁵ are included for comparison. The experimental diffusion coefficients are indicated by green up-triangles⁹⁶ and cyan left-triangle⁹⁷. (b) Same as (a) for D_2O . Results from PIMD simulations using the q-TIP4P/F model are shown with red circles. Green circles indicates the diffusion coefficient for the same water model from classical MD simulations. For comparison, we include the diffusion coefficient of q-TIP4P/F heavy water at $T = 300$ K from PIMD simulations (red square) reported in Ref. ⁶⁵. The experimental diffusion coefficients for heavy water are indicated by orange up-triangles, from Ref. ⁹⁸. The insets in (a) and (b) are the ratio of the diffusion coefficients obtained from PIMD and MD simulations.

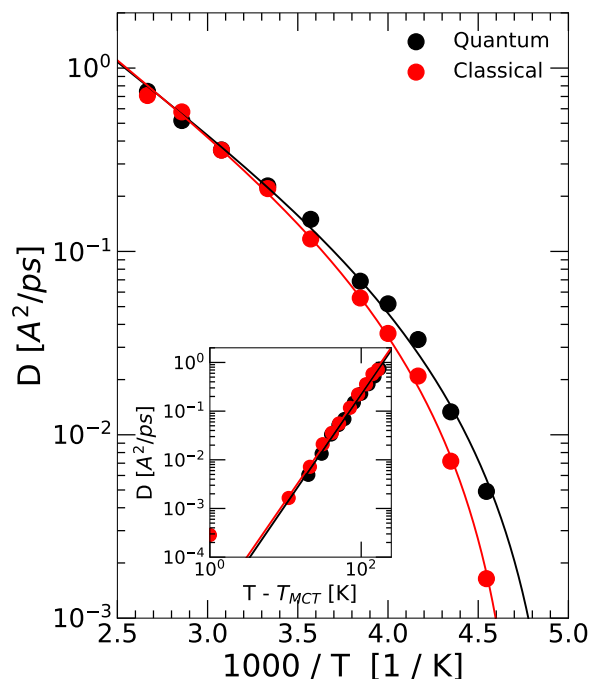


Fig. 7 Diffusion coefficient of q-TIP4P/F water as a function of temperature at $P = 1$ bar from PIMD simulations (black) and classical MD simulations (red). Solid lines are the best fit using Eq. 9, as predicted from MCT. The corresponding fitting parameters are ($T_{MCT} = 200$ K, $\gamma = 2.27$) from PIMD simulations (for $T \geq 220$ K) and ($T_{MCT} = 209$ K and $\gamma = 2.25$) from classical MD simulations (for $T \geq 220$ K). Inset: Same as main panel in a log-log scale plot.

putational works using various water models suggest that the ratio $R = D_{NQE}/D_{noNQE} = 1.15 - 1.50$ at $T = 300$ K⁶⁵, where D_{NQE} (D_{noNQE}) is the water diffusion coefficient when NQE are (are not) included. However, Habershon *et al.* find that for q-TIP4P/F water R is much smaller, $R = 1.15$ at $T = 300$ K (in Ref. ¹⁰¹, it was found that $R = 1.07$ for a small system of $N = 125$ molecules). As shown in the inset of Fig. 6, our results at $T = 300$ K are consistent with this value, $R \approx 1.04$. However, at lower temperatures, R increases considerably, e.g., $R > 3$ at $T \leq 220$ K. Indeed, it follows from the MCT fits shown in Fig. 7 that R should exhibit an apparent divergency as the MCT temperature of the classical model is approached ($T \approx 209$ K). However, since MCT fails at approximately $T \leq T_{MCT}$, the apparent divergency in R does not occur.

3.3 Structure

To characterize the structure of H_2O and D_2O from our PIMD simulations, we focus on the following properties, (i) OO, OH, and HH radial distribution functions (RDF), (ii) water molecules OH length and HOH angle distributions, and (iii) the corresponding local tetrahedral order parameter q defined in Ref. ¹⁰². In order to interpret these properties appropriately, it is important to understand how delocalized the H/D and O atoms are. Accordingly, first, we calculate the distance r_{bc} from the bead of a given ring-polymer to the corresponding ring-polymer center of mass. Fig. 8, shows the probability distribution of r_{bc} for the O

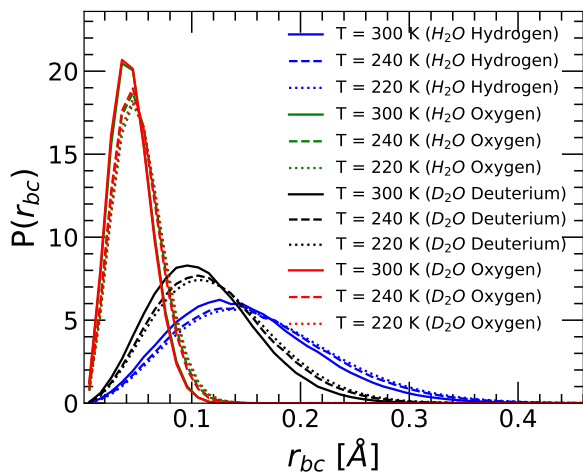


Fig. 8 Probability distribution $P(r_{bc})$ to find a bead of a given ring polymer at a distance r_{bc} from the corresponding centroid. Probability distributions are calculated for H_2O and D_2O oxygen and hydrogen/deuterium atoms. Hydrogen atoms can be considerably delocalized with the associated ring-polymer beads being displaced by as much as 0.4 \AA (40% of the OH covalent bond length) from the corresponding ring-polymer center of mass. The area under each curve is normalized to unity.

and H/D atoms of the water molecules. As expected, the lighter the atom, the more delocalized it is. Specifically, the beads of the ring-polymer associated to the O atom can spread up to only 0.1 \AA (10 % of the OH covalent bond length) from the corresponding ring-polymer center of mass. Instead, in the case of H atoms, beads can be found as far as $0.35 - 0.4 \text{ \AA}$ away from the corresponding ring-polymer center of mass. This implies that the H atoms can be thought of a "cloud" with diameter $d \approx 0.7 - 0.8 \text{ \AA}$, comparable to the OH covalent bond length (in the case of D atoms, $d \approx 0.55 - 0.60 \text{ \AA}$). Not surprisingly, nuclear fluctuations should play a relevant role in atomic interactions involving H and D. Interestingly, the atoms delocalization due to NQE is mildly dependent on temperature for $T = 350 - 220 \text{ K}$.

(i) The HH, OH, and OO RDF of q-TIP4P/F water are shown in Fig. 9 for selected temperatures. For comparison, we also include the RDF of the classical version of q-TIP4P/F water ($n_b = 1$). Our RDF at $T = 300 \text{ K}$ are consistent with those reported by Habershon et. al. in Ref.⁶⁵ and, in particular, with experiments. For example, the first and second peaks of the OO RDF are located at $\approx 0.28 \text{ nm} \approx 0.45 \text{ nm}$, which are characteristic of the tetrahedral local structure of water. Similarly, the first peak of the OH RDF is located at $\approx 0.18 \text{ nm}$ which is characteristic of the water-water hydrogen bond. In addition, as expected, the main effect of lowering the temperature is to enhanced the local structure of water, making water a more tetrahedral liquid (see below). Regarding the NQE, Fig. 9 shows that adding NQE tends to smooth out the maxima of the RDF, relative to the classical version of q-TIP4P/F water. In other words, as shown in previous PIMD simulations^{103,104}, adding NQE to a classical water model makes water less structured. Indeed, consistent with Ref.¹⁰⁵, the RDFs of H_2O at temperature $T = 300 \text{ K}$ from PIMD simulations practically overlap with the RDFs obtained from classical MD simulation at

temperature $T + \Delta T$ where $\Delta T = +25 \text{ K}$.

The structure of heavy water is shown in Fig. 10. Briefly, the structures of D_2O and H_2O are very similar. As shown in Figs. 10(a) and 10(b), the RDF of heavy water are slightly sharper, i.e., D_2O is more structured than H_2O . This is consistent with the fact that D atoms are more localized than H atoms (Fig. 8).

(ii) Figs. 11(a) and 11(b) show the probability distribution of the OH covalent bond length r_{OH} and HOH angle θ_{HOH} of the q-TIP4P/F water molecules at different temperatures. The OH length and HOH angle distributions are obtained by averaging (over all molecules and time) the following estimators

$$\tilde{d}_{OH} = \frac{1}{n_b} \sum_{k=1}^{n_b} d_{OH,k} \quad \text{and} \quad \tilde{\theta}_{HOH} = \frac{1}{n_b} \sum_{k=1}^{n_b} \theta_{HOH,k} \quad (10)$$

where $d_{OH,k}$ and $\theta_{HOH,k}$, are the OH distance and HOH angle of molecules in replica k . When the centroids of the oxygen and hydrogen ring-polymers are used, the OH and HOH distributions practically coincide with those obtained from the classical MD simulations.

The probability distributions for r_{OH} , $P(r_{OH})$, is centered at $r_{OH} \approx 0.97 \text{ nm}$ (blue lines) for quantum H_2O and $\approx 0.95 \text{ nm}$ (black lines) for classical H_2O . Hence, NQE tend to stretch the OH distance covalent bond length. Interestingly, the classical and quantum distributions in Fig. 11a have the same shape meaning that the fluctuations of r_{OH} for the quantum and classical case for q-TIP4P/F water are remarkably similarly.

Surprisingly, the $P(\theta_{HOH})$ distribution functions for quantum and classical q-TIP4P-F water are practically identical, i.e., NQE do not change the fluctuations or average value of the HOH angle. The average θ_{HOH} for the quantum and classical case is 105° . Since the average r_{OH} distance is different in the quantum and classical case, while θ_{HOH} is not, it follows that NQE must affect the molecular dipole moment μ ; see Fig. 11(c). NQE shift the maximum of the dipole moment in classical q-TIP4P/F water from ≈ 2.3 to ≈ 2.35 . The small differences in μ , may also explain why the dielectric constant ϵ (see Fig. 5) is very similar for quantum and classical q-TIP4P/F water.

Fig. 11 also shows the results obtained from our PIMD simulations of D_2O using the q-TIP4P/F model. Overall, the differences in r_{OH} , θ_{HOH} , and μ between H_2O and D_2O are rather minor. For both (quantum and classical) H_2O and D_2O , the corresponding distributions show minor variations with temperature; decreasing the temperature leads to sharper distribution functions.

(iii) An important property of supercooled water is its rapid increase of tetrahedrality upon supercooling at $P = 1 \text{ bar}$. To quantify the local tetrahedrality of q-TIP4P/F light and heavy water, we calculate the local order parameter q defined in Ref.¹⁰². For a classical system, the local order parameter q_i of molecule i is defined as

$$q_i = 1 - \frac{3}{8} \sum_{j=1}^3 \sum_{k=j+1}^4 \left(\cos \psi_{ijk} + \frac{1}{3} \right)^2 \quad (11)$$

where ψ_{ijk} is the angle formed by the lines joining the oxygen atom of molecule i and the O atoms of its nearest neighbors j and k . The local order parameter of the system q is obtained

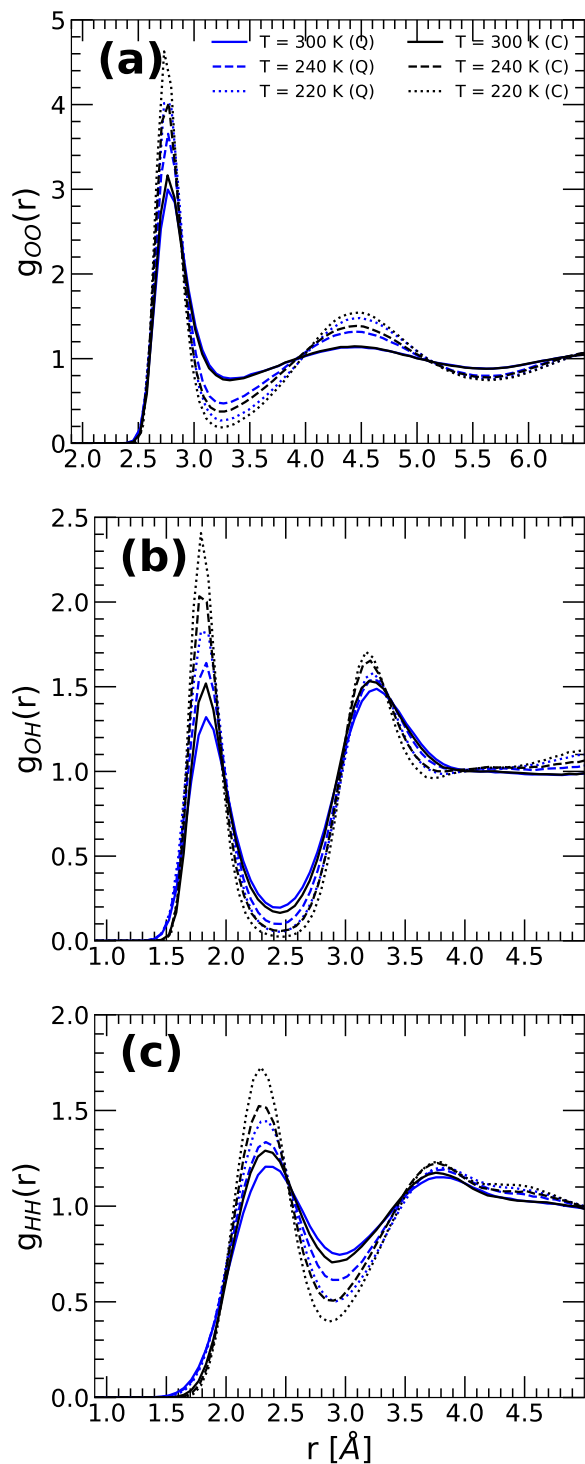


Fig. 9 (a) Oxygen-oxygen, (b) oxygen-hydrogen and (c) hydrogen-hydrogen RDF of H_2O obtained from PIMD (blue lines) and classical MD simulations (black lines) using the q-TIP4P/F model. With decreasing temperatures, the maxima in the OO, OH, and HH RDF become more pronounced in the classical case meaning the water molecule atoms are less structured as NQE are included.

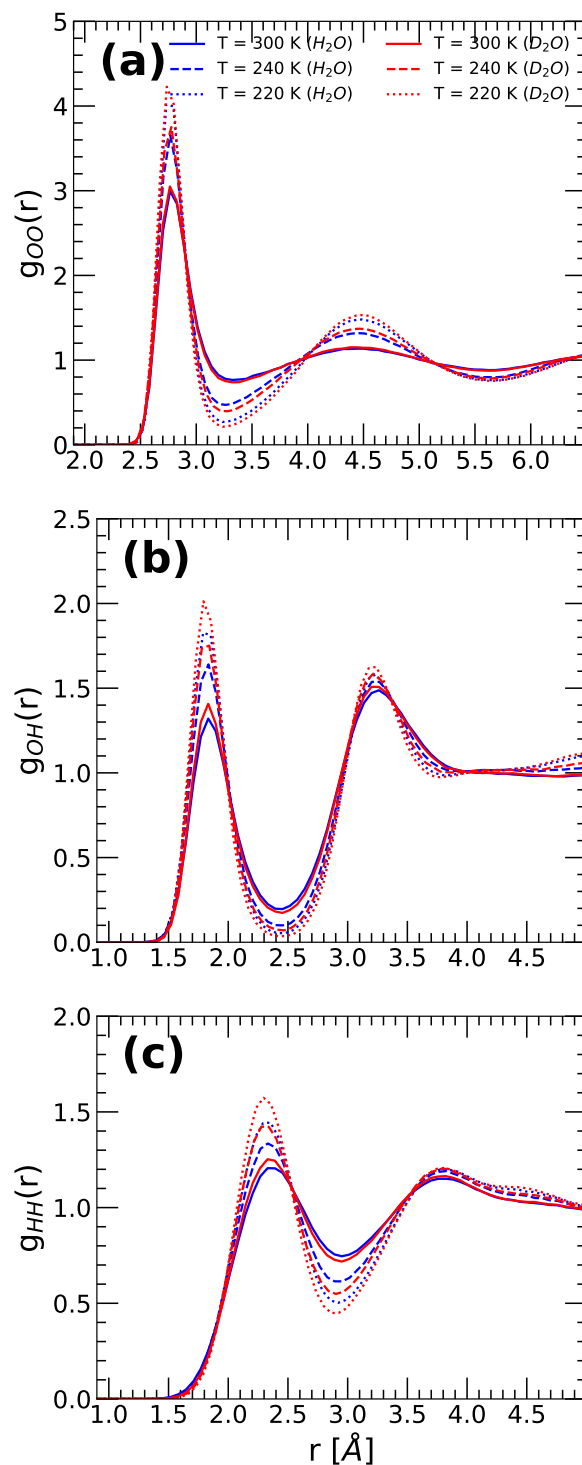


Fig. 10 (a) Oxygen-oxygen, (b) oxygen-hydrogen and (c) hydrogen-hydrogen RDF of H_2O (blue lines) and D_2O (red lines) obtained from PIMD simulations using the qTIP4P/F model. H_2O is less structured than D_2O since atom delocalization due to NQE are more pronounced for hydrogen atoms than for deuterium atoms.

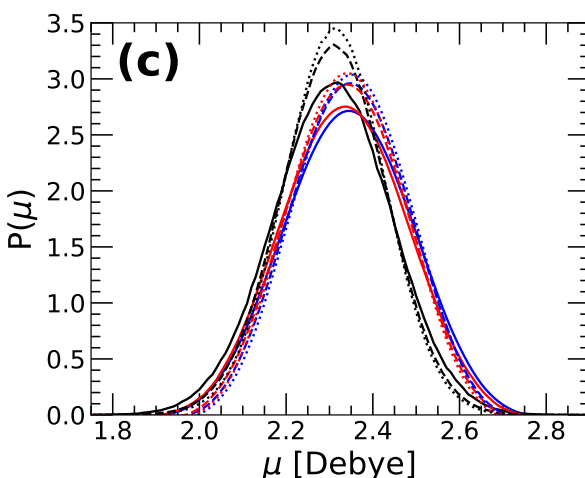
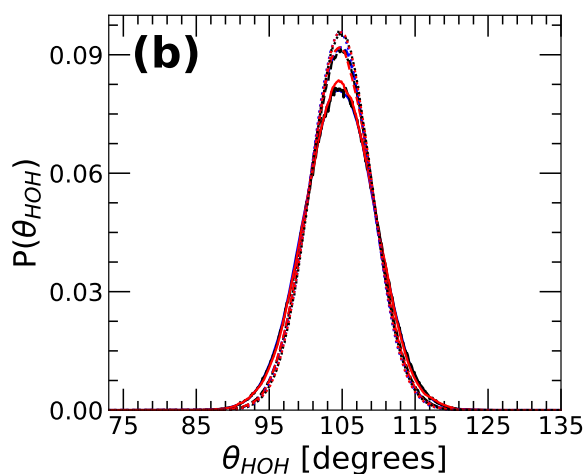
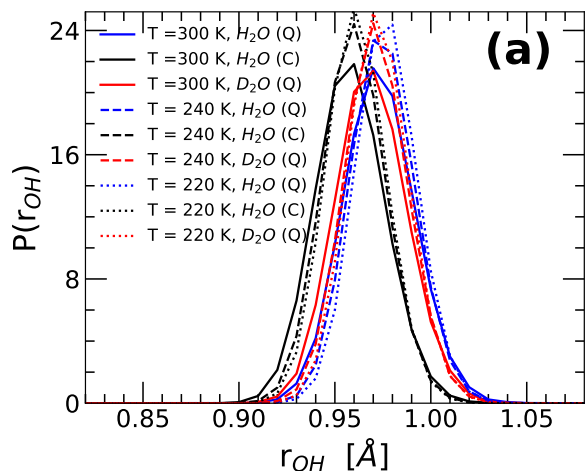


Fig. 11 Probability distribution function for (a) the OH/OD covalent-bond length of H_2O and D_2O molecules, (b) the HOH/DOD bond angle, and (c) the molecular dipole moment, at selected temperatures. Results are from PIMD simulations (H_2O , blue lines; D_2O , red lines) and classical MD simulations (H_2O , black lines). Distributions calculated using the centroids of the water atoms practically coincide with the classical results (not shown).

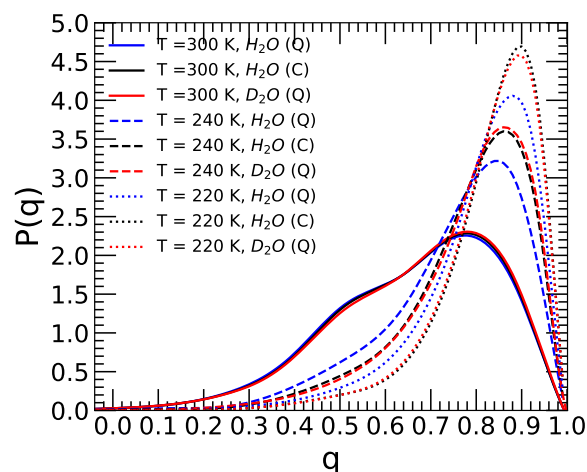


Fig. 12 Probability distribution of the tetrahedral order parameter q for H_2O and D_2O . Results from PIMD simulations for H_2O and D_2O using the q -TIP4P/F model are shown by blue and red lines; black lines are results for H_2O from classical MD simulations using the same water model. At low temperatures, H_2O and D_2O are highly tetrahedral and $P(q)$ exhibits a maximum at large q . As the temperature increases, a shoulder develops at low q , indicating the appearance of a new family of molecules with weakly tetrahedral local arrangements.

by averaging q_i over all the molecules. For a perfect tetrahedral network (e.g., hexagonal ice), $q = 1$; for a random distribution of molecules, the average value of q is zero. We use the same definition of q for the case of PIMD simulations. However, the local tetrahedral order parameter for molecule i is calculated by averaging over all the replicas,

$$q_i = \frac{1}{n_b} \sum_{k=1}^{n_b} q_{i,k} \quad (12)$$

where $q_{i,k}$ is given by Eq. 11 with all O atoms belonging to replica k .

The probability distribution of the tetrahedral order parameter $P(q)$ for H_2O and D_2O , from classical MD and PIMD simulations using the q -TIP4P/F model, are shown in Fig. 12. Consistent with early classical MD simulations of water, in all cases, $P(q)$ indicates the presence of two local arrangements of water molecules at high temperature. The large- q (low- q) family of molecules are in highly-tetrahedral (weakly-tetrahedral) environments. In addition, upon cooling, the large- q peak grows and shifts towards larger values of q , while the low- q family of water disappears, suggesting that water becomes more tetrahedral as defects of the hydrogen-bond network of water vanish. The picture that emerges from Fig. 12 is consistent with scenarios where water is composed of two distinct local arrangements (see, e.g., Refs.^{5,6,8,106}) and, in particular, with the LLC hypothesis scenario. Hence, the presence of NQE does not exclude the LLC hypothesis scenario as a possible framework to explain the anomalous behavior of water at low temperatures.

4 Conclusions

We studied the properties of H_2O and D_2O at atmospheric pressure and for temperatures extending from the equilibrium to the supercooled liquid states. Our study is based on PIMD simulations using the q-TIP4P/F flexible water model where nuclear quantum effects are included. Computational studies of the thermodynamic and dynamical properties of water in equilibrium and supercooled liquid states are available at $P = 1$ atm. However, most of these studies are based on classical computer simulations employing rigid water models where nuclear quantum effects are omitted. The few studies based on PIMD simulations (and other quantum simulation techniques) have been limited to a few properties evaluated usually at a few equilibrium states (e.g., $T = 300$ K and $P = 1$ atm). Accordingly, it is unclear from the available studies whether PIMD simulations can reproduce the thermodynamic and dynamic properties of water in the P-T phase diagram. In this work, we focus on various (a) thermodynamic, (b) dynamical, and structural properties of H_2O and D_2O .

(a) From the thermodynamic point of view, our results show that PIMD simulations of H_2O and D_2O based on the q-TIP4P/F model reproduce successfully the available experimental $\rho(T)$ (for approximately $T \geq 240$ K). Deviations relative to experiments are < 0.005 and < 0.01 g/cm³ for H_2O and D_2O (0.5 % and 1.0 %). We also study the following thermodynamic response functions $\alpha_P(T)$, $\kappa_T(T)$, $C_P(T)$, and $\epsilon(T)$. These thermodynamic properties quantify, respectively, cross-correlations in entropy and volume, and fluctuations in volume, entropy, and dipole moment^{107,108}. We find that, in equilibrium ($T \geq 273$ K in the case of H_2O), PIMD simulations are in remarkably good quantitative agreement with experiments for the case of $\alpha_T(T)$ and $\kappa_T(T)$ (with deviations relative to experiments of 1 - 10 %), while qualitative agreement is found in the case of $C_P(T)$ and $\epsilon(T)$ (deviations relative to experiments can be as large as 5 - 30 %). The case of $C_P(T)$ should be taken with caution since, as shown in the SM, the evaluation of $C_P(T)$ from the corresponding enthalpy is very sensitive to details of the PIMD simulations, including the simulation time step (dt) and number of beads per ring-polymer ($n_b \geq 32$) employed. Overall, our PIMD simulations of H_2O and D_2O based on the q-TIP4P/F model provide thermodynamic properties that are quantitatively or semi-quantitatively consistent with experiments in the equilibrium state.

The situation is different in the supercooled domain ($T < 273$ K in the case of H_2O). At these temperatures, PIMD simulations show a systematic underestimation of $\alpha_T(T)$, $\kappa_T(T)$, $C_P(T)$, and $\epsilon(T)$ for both H_2O and D_2O which become more pronounced upon supercooling. This indicates that the PIMD simulations of q-TIP4P/F water, although including nuclear quantum effects, are not able to reproduce the fluctuations in volume, entropy, and electric dipole moment observed in real water. Some sources of fluctuations are missing in the flexible q-TIP4P/F model; similar conclusions were obtained in Ref.¹⁰⁹ for the case of classical water models. It is not clear whether these problems can be solved by introducing polarizability to the q-TIP4P/F model or whether other contributions, such as three-body interactions are needed. The underestimation of fluctuations in classical water models is

common, however, we show here that nuclear quantum effects, alone, may not be sufficient to reproduce the fluctuations in real water.

One of the most important open questions in supercooled light and heavy water is whether they exhibit a LLCP at low temperatures. A LLCP is found in classical computer simulations of H_2O using the ST2, TIP4P/ice, and TIP4P/2005 water at $P > 1$ bar. These studies also show that the presence of a LLCP in water leads to a maximum in $\kappa_T(T)$ ^{32,82} at $P = 1$ bar and simulations show that a maximum in $C_P(T)$ at $P = 1$ bar should exist as well⁸¹. The TIP4P/2005 and TIP4P/ice model are among the (rigid) models that best reproduce the properties of liquid water and ice in the P-T plane. Since the (flexible) q-TIP4P/F model used in this work has been parameterized based on the TIP4P/2005 model [61], one would expect to find a maximum in $\kappa_T(T)$. Indeed, we find a maximum in $\kappa_T(T)$ in PIMD and classical MD simulations. The maximum from our PIMD and classical MD simulations for H_2O and D_2O occurs at $T \approx 230$ K and $T \approx 235$ K, respectively, consistent with the experimentally observed maximum ($T = 228$ K and $T = 233$ K¹¹). We also note that a maximum in $C_P(T)$ at $P = 1$ bar is not found either in the classical MD ($T \geq 200$ K) or PIMD simulations ($T \geq 210$ K) of q-TIP4P/F light and heavy water, while such a maximum in C_P has been reported in a recent experiment⁵⁸. Overall, the present simulations show a picture that is not inconsistent with the LLCP scenario for water although additional simulations are required to confirm the existence of a LLCP in supercooled q-TIP4P/F water from PIMD simulations. Interestingly, we find that the $\rho(T)$, $\kappa_T(T)$, and $\alpha_P(T)$ obtained from classical MD and PIMD simulations of q-TIP4P/F H_2O and D_2O water practically overlap.

(b) From the dynamical point of view, we find that the diffusion coefficients of H_2O and D_2O obtained from PIMD simulations are in excellent agreement with experimental values ($T > 230$ K); see Fig. 6. Interestingly, compared to classical MD simulations, NQE practically do not enhance the diffusion coefficient of water at $T > 270$ K. For example, $D_Q(T)/D_C(T) \approx 1.05$ at $T = 300$ K, where $D_Q(T)$ and $D_C(T)$ are the diffusion coefficients of water from PIMD and classical MD simulations; Habershon *et al.* find similar values, $D_Q(T)/D_C(T) \approx 1.07 - 1.15$ ⁶⁵. However, NQE play a relevant role in the dynamics of supercooled water with $D_Q(T)/D_C(T) > 3$ at $T \leq 220$ K. Such an increase in the diffusivity of supercooled water due to NQE may be important in the determination of the glass transition temperature of H_2O and D_2O in computational/theoretical studies.

(c) We also discussed the NQE effects on the structure of H_2O and D_2O . As shown in previous works, relative to classical MD simulations, including NQE makes H_2O and D_2O less structured with smaller maxima in the radial distribution functions. This is because NQE make the H and D atoms delocalized. For example, the ring-polymer beads associated to the H (D) atom are displaced by as much as ≈ 0.4 Å (≈ 0.3 Å) from the corresponding centroid. These are relevant distances compared with the OH covalent bond length ≈ 1 Å.

Our results also show that water molecules seems to exist in two different kinds of local arrangements. At high temperatures, molecules are in two kinds of local arrangements with low and

high degree of tetrahedrality. However, with decreasing temperatures, molecules can be found mostly in highly-tetrahedral local arrangements. The presence of two kinds of local structural environments is postulated by different scenarios to explain water anomalous behavior and it is supported by most computer simulations of rigid (classical) water models^{8,31,106,110}. The existence of two "kinds of water" is consistent with the LLCP hypothesis scenario for water⁵.

5 Conflicts of Interest

There are no conflicts to declare.

6 Acknowledgments

We thank P. Eastman for help with the OpenMM software package. This work was supported, in part, by a grant of computer time from the City University of New York High Performance Computing Center under NSF Grants CNS-0855217, CNS-0958379 and ALI-1126113. We acknowledge support from the NSF CREST Center for Interface Design and Engineered Assembly of Low Dimensional systems (IDEALS), NSF grant number HRD-1547380.

Notes and references

- 1 Y. Levy and J. N. Onuchic, *Annu. Rev. Biophys. Biomol. Struct.*, 2006, **35**, 389–415.
- 2 F. Franks, *Water: a matrix of life*, Royal Society of Chemistry, 2007.
- 3 P. G. Debenedetti, *Metastable liquids: concepts and principles*, Princeton university press, 1996, vol. 1.
- 4 P. G. Debenedetti, *J. Phys.: Condens. Matter*, 2003, **15**, R1669.
- 5 P. Gallo, K. Amann-Winkel, C. A. Angell, M. A. Anisimov, F. Caupin, C. Chakravarty, E. Lascaris, T. Loerting, A. Z. Panagiotopoulos, J. Russo *et al.*, *Chem. Rev.*, 2016, **116**, 7463–7500.
- 6 O. Mishima and H. E. Stanley, *Nature (London)*, 1998, **396**, 329–335.
- 7 C. A. Angell, *Science*, 2008, **319**, 582–587.
- 8 A. Nilsson and L. G. Pettersson, *Nat. Commun.*, 2015, **6**, 1–11.
- 9 J. A. Sellberg, C. Huang, T. A. McQueen, N. Loh, H. Laksmono, D. Schlesinger, R. Sierra, D. Nordlund, C. Hampton, D. Starodub *et al.*, *Nature (London)*, 2014, **510**, 381–384.
- 10 P. G. Debenedetti and H. E. Stanley, *Phys. Today*, 2003, **56**, 40–46.
- 11 K. H. Kim, A. Späh, H. Pathak, F. Perakis, D. Mariedahl, K. Amann-Winkel, J. A. Sellberg, J. H. Lee, S. Kim, J. Park *et al.*, *Science*, 2017, **358**, 1589–1593.
- 12 A. Späh, H. Pathak, K. H. Kim, F. Perakis, D. Mariedahl, K. Amann-Winkel, J. A. Sellberg, J. H. Lee, S. Kim, J. Park *et al.*, *Phys. Chem. Chem. Phys.*, 2019, **21**, 26–31.
- 13 P. H. Handle, T. Loerting and F. Sciortino, *Proc. Natl. Acad. Sci.*, 2017, **114**, 13336–13344.
- 14 P. H. Poole, F. Sciortino, U. Essmann and H. E. Stanley, *Nature (London)*, 1992, **360**, 324–328.
- 15 O. Mishima and H. E. Stanley, *Nature (London)*, 1998, **392**, 164–168.
- 16 O. Mishima, *J. Chem. Phys.*, 2010, **133**, 144503.
- 17 H. Pathak, A. Späh, K. Amann-Winkel, F. Perakis, K. K. H. Kim and A. Nilsson, *Mol. Phys.*, 2019, **117**, 3232–3240.
- 18 T. Loerting and N. Giovambattista, *J. Phys.: Condens. Matter*, 2006, **18**, R919.
- 19 O. Mishima, L. Calvert and E. Whalley, *Nature (London)*, 1984, **310**, 393–395.
- 20 O. Mishima, L. Calvert and E. Whalley, *Nature (London)*, 1985, **314**, 76–78.
- 21 C. A. Angell, *Annu. Rev. Phys. Chem.*, 2004, **55**, 559–583.
- 22 K. Amann-Winkel, R. Böhmer, F. Fujara, C. Gainaru, B. Geil and T. Loerting, *Rev. Mod. Phys.*, 2016, **88**, 011002.
- 23 K. H. Kim, K. Amann-Winkel, N. Giovambattista, A. Späh, F. Perakis, H. Pathak, M. L. Parada, C. Yang, D. Mariedahl, T. Eklund *et al.*, *Sci.*, 2020, **370**, 978–982.
- 24 J. Wong, D. A. Jahn and N. Giovambattista, *J. Chem. Phys.*, 2015, **143**, 074501.
- 25 J. Engstler and N. Giovambattista, *J. Chem. Phys.*, 2017, **147**, 074505.
- 26 N. Giovambattista, T. Loerting, B. R. Lukanov and F. W. Starr, *Sci. Rep.*, 2012, **2**, 1–8.
- 27 N. Giovambattista, *Adv. Chem. Phys.*, 2013, **152**, 113.
- 28 N. Giovambattista, F. W. Starr and P. H. Poole, *J. Chem. Phys.*, 2019, **150**, 224502.
- 29 F. Martelli, N. Giovambattista, S. Torquato and R. Car, *Phys. Rev. Mater.*, 2018, **2**, 075601.
- 30 P. H. Handle, F. Sciortino and N. Giovambattista, *J. Chem. Phys.*, 2019, **150**, 244506.
- 31 R. S. Singh, J. W. Biddle, P. G. Debenedetti and M. A. Anisimov, *J. Chem. Phys.*, 2016, **144**, 144504.
- 32 M. A. González, C. Valeriani, F. Caupin and J. L. Abascal, *J. Chem. Phys.*, 2016, **145**, 054505.
- 33 G. Pallares, M. E. M. Azouzi, M. A. González, J. L. Aragones, J. L. Abascal, C. Valeriani and F. Caupin, *Proc. Natl. Acad. Sci.*, 2014, **111**, 7936–7941.
- 34 O. Mishima, *J. Chem. Phys.*, 1994, **100**, 5910–5912.
- 35 J. N. Stern, M. Seidl-Nigsch and T. Loerting, *Proc. Natl. Acad. Sci.*, 2019, **116**, 9191–9196.
- 36 Y. Suzuki, *J. Chem. Phys.*, 2019, **150**, 224508.
- 37 C. A. Tulk, J. J. Molaison, A. R. Makhlof, C. E. Manning and D. D. Klug, *Nature (London)*, 2019, **569**, 542–545.
- 38 T. Strässle, A. Saitta, S. Klotz and M. Braden, *Phys. Rev. Lett.*, 2004, **93**, 225901.
- 39 T. Strässle, S. Klotz, G. Hamel, M. M. Koza and H. Schober, *Phys. Rev. Lett.*, 2007, **99**, 175501.
- 40 Y. Wang, H. Zhang, X. Yang, S. Jiang and A. F. Goncharov, *J. Chem. Phys.*, 2018, **148**, 044508.
- 41 C. Lin, X. Yong, S. T. John, J. S. Smith, S. V. Sinogeikin, C. Kenney-Benson and G. Shen, *Phys. Rev. Lett.*, 2017, **119**, 135701.

- 42 J. Tse, D. Klug, C. Tulk, I. Swainson, E. Svensson, C.-K. Loong, V. Shpakov, V. Belosludov, R. Belosludov and Y. Kawazoe, *Nature (London)*, 1999, **400**, 647–649.
- 43 T. E. Gartner, L. Zhang, P. M. Piaggi, R. Car, A. Z. Panagiotopoulos and P. G. Debenedetti, *Proc. Natl. Acad. Sci.*, 2020, **117**, 26040–26046.
- 44 J. C. Palmer, F. Martelli, Y. Liu, R. Car, A. Z. Panagiotopoulos and P. G. Debenedetti, *Nature (London)*, 2014, **510**, 385–388.
- 45 J. C. Palmer, R. Car and P. G. Debenedetti, *Faraday Discuss.*, 2013, **167**, 77–94.
- 46 J. C. Palmer, P. H. Poole, F. Sciortino and P. G. Debenedetti, *Chem. Rev.*, 2018, **118**, 9129–9151.
- 47 Y. Liu, J. C. Palmer, A. Z. Panagiotopoulos and P. G. Debenedetti, *J. Chem. Phys.*, 2012, **137**, 214505.
- 48 P. H. Poole, I. Saika-Voivod and F. Sciortino, *J. Phys.: Condens. Matter*, 2005, **17**, L431.
- 49 P. H. Handle and F. Sciortino, *J. Chem. Phys.*, 2018, **148**, 134505.
- 50 P. H. Poole, R. K. Bowles, I. Saika-Voivod and F. Sciortino, *J. Chem. Phys.*, 2013, **138**, 034505.
- 51 P. G. Debenedetti, F. Sciortino and G. H. Zerze, *Science*, 2020, **369**, 289–292.
- 52 A. Scala, F. W. Starr, E. La Nave, H. E. Stanley and F. Sciortino, *Phys. Rev. E*, 2000, **62**, 8016–8020.
- 53 E. B. Moore and V. Molinero, *Nature (London)*, 2011, **479**, 506–508.
- 54 J. L. Abascal and C. Vega, *J. Chem. Phys.*, 2005, **123**, 234505.
- 55 K. Amann-Winkel, C. Gainaru, P. H. Handle, M. Seidl, H. Nelson, R. Bohmer and T. Loerting, *Proc. Natl. Acad. Sci.*, 2013, **110**, 17720–17725.
- 56 V. Holten, C. Qiu, E. Guillermin, M. Wilke, J. Ricka, M. Frenz and F. Caupin, *J. Phys. Chem. Lett.*, 2017, **8**, 5519–5522.
- 57 L. Kringle, W. A. Thornley, B. D. Kay and G. A. Kimmel, *Sci.*, 2020, **369**, 1490–1492.
- 58 H. Pathak, A. Späh, N. Esmaeildoost, J. A. Sellberg, K. H. Kim, F. Perakis, K. Amann-Winkel, M. Ladd-Parada, J. Koliyadu, T. J. Lane *et al.*, *Proc. Natl. Acad. Sci.*, 2021, **118**, year.
- 59 M. Ceriotti, W. Fang, P. G. Kusalik, R. H. McKenzie, A. Michaelides, M. A. Morales and T. E. Markland, *Chem. Rev.*, 2016, **116**, 7529–7550.
- 60 C. Gainaru, A. L. Agapov, V. Fuentes-Landete, K. Amann-Winkel, H. Nelson, K. W. Köster, A. I. Kolesnikov, V. N. Novikov, R. Richert, R. Böhmer *et al.*, *Proc. Natl. Acad. Sci.*, 2014, **111**, 17402–17407.
- 61 O. Mishima and H. E. Stanley, *Nature (London)*, 1998, **392**, 164–168.
- 62 O. Mishima, *Phys. Rev. Lett.*, 2000, **85**, 334–336.
- 63 B. Nguyen, G. E. Lopez and N. Giovambattista, *Phys. Chem. Chem. Phys.*, 2018, **20**, 8210–8217.
- 64 Y. Liu, G. Sun, A. Eltareb, G. E. Lopez, N. Giovambattista and L. Xu, *Phys. Rev. Res.*, 2020, **2**, 013153.
- 65 S. Habershon, T. E. Markland and D. E. Manolopoulos, *J. Chem. Phys.*, 2009, **131**, 024501.
- 66 S. K. Reddy, S. C. Straight, P. Bajaj, C. Huy Pham, M. Rivera, D. R. Moberg, M. A. Morales, C. Knight, A. W. Götz and F. Paesani, *J. Chem. Phys.*, 2016, **145**, 194504.
- 67 B. Cheng, E. A. Engel, J. Behler, C. Dellago and M. Ceriotti, *Proc. Natl. Acad. Sci.*, 2019, **116**, 1110–1115.
- 68 O. Marsalek and T. E. Markland, *J. Phys. Chem. Lett.*, 2017, **8**, 1545–1551.
- 69 R. Ramírez and C. Herrero, *Phys. Rev. B*, 2011, **84**, 064130.
- 70 R. Ramírez, N. Neuerburg, M.-V. Fernandez-Serra and C. Herrero, *J. Chem. Phys.*, 2012, **137**, 044502.
- 71 P. Eastman, M. S. Friedrichs, J. D. Chodera, R. J. Radmer, C. M. Bruns, J. P. Ku, K. A. Beauchamp, T. J. Lane, L.-P. Wang, D. Shukla *et al.*, *J. Chem. Theory Comput.*, 2013, **9**, 461–469.
- 72 S. Habershon and D. E. Manolopoulos, *Phys. Chem. Chem. Phys.*, 2011, **13**, 19714.
- 73 M. Ceriotti, M. Parrinello, T. E. Markland and D. E. Manolopoulos, *J. Chem. Phys.*, 2010, **133**, 124104.
- 74 T. E. Markland and D. E. Manolopoulos, *J. Chem. Phys.*, 2008, **129**, 024105.
- 75 J. Liu, W. H. Miller, F. Paesani, W. Zhang and D. A. Case, *J. Chem. Phys.*, 2009, **131**, 164509.
- 76 L. Ruiz Pestana, O. Marsalek, T. E. Markland and T. Head-Gordon, *J. Phys. Chem. Lett.*, 2018, **9**, 5009–5016.
- 77 G. Kell, *J. Chem. Eng. Data*, 1967, **12**, 66–69.
- 78 D. Hare and C. Sorensen, *J. Chem. Phys.*, 1987, **87**, 4840–4845.
- 79 D. Hare and C. Sorensen, *J. Chem. Phys.*, 1986, **84**, 5085–5089.
- 80 R. Pathria and P. D. Beale, *New York*, 2011.
- 81 S. V. Buldyrev, G. Malescio, C. A. Angell, N. Giovambattista, S. Prestipino, F. Saija, H. E. Stanley and L. Xu, *J. Phys.: Condens. Matter*, 2009, **21**, 504106.
- 82 J. L. Abascal and C. Vega, *J. Chem. Phys.*, 2010, **133**, 234502.
- 83 F. J. Millero and F. K. Lepple, *J. Chem. Phys.*, 1971, **54**, 946–949.
- 84 C. Vega, M. M. Conde, C. McBride, J. L. F. Abascal, E. G. Noya, R. Ramírez and L. M. Sesé, *J. Chem. Phys.*, 2010, **132**, 046101.
- 85 M. Shiga and W. Shinoda, *J. Chem. Phys.*, 2005, **123**, 134502.
- 86 C. Angell, W. Sichina and M. Oguni, *J. Phys. Chem.*, 1982, **86**, 998–1002.
- 87 I. Hodge and C. Angell, *J. Chem. Phys.*, 1978, **68**, 1363–1368.
- 88 R. Speedy and C. Angell, *J. Chem. Phys.*, 1976, **65**, 851–858.
- 89 C. Malmberg and A. Maryott, *J. Res. Natl. Bur. Stand. (U. S.)*, 1956, **56**, 1.
- 90 C. G. Malmberg, *J. Res. Natl. Bur. Stand.*, 1958, **60**, year.
- 91 I. R. Craig and D. E. Manolopoulos, *J. Chem. Phys.*, 2004, **121**, 3368–3373.
- 92 S. Habershon, D. E. Manolopoulos, T. E. Markland and T. F.

- Miller III, *Annu. Rev. Phys. Chem.*, 2013, **64**, 387–413.
- 93 T. F. Miller III, *J. Chem. Phys.*, 2008, **129**, 194502.
- 94 M. Rossi, M. Ceriotti and D. E. Manolopoulos, *J. Chem. Phys.*, 2014, **140**, 234116.
- 95 I.-C. Yeh and G. Hummer, *J. Phys. Chem. B*, 2004, **108**, 15873–15879.
- 96 W. S. Price, H. Ide and Y. Arata, *J. Phys. Chem. A*, 1999, **103**, 448–450.
- 97 M. Holz, S. R. Heil and A. Sacco, *Phys. Chem. Chem. Phys.*, 2000, **2**, 4740–4742.
- 98 W. S. Price, H. Ide, Y. Arata and O. Söderman, *J. Phys. Chem. B*, 2000, **104**, 5874–5876.
- 99 R. Torre, P. Bartolini and R. Righini, *Nature (London)*, 2004, **428**, 296–299.
- 100 W. Götze, *In Les Houches Summer Schools of Theoretical Physics Session LI (1989)*; JP Hansen, D. Levesque, J. Zinn-Justin, Eds, 1991.
- 101 S. Habershon and D. E. Manolopoulos, *J. Chem. Phys.*, 2009, **131**, 244518.
- 102 J. R. Errington and P. G. Debenedetti, *Nature (London)*, 2001, **409**, 318–321.
- 103 H. A. Stern and B. Berne, *J. Chem. Phys.*, 2001, **115**, 7622–7628.
- 104 F. Paesani, W. Zhang, D. A. Case, T. E. Cheatham III and G. A. Voth, *J. Chem. Phys.*, 2006, **125**, 184507.
- 105 J. A. Morrone and R. Car, *Phys. Rev. Lett.*, 2008, **101**, 017801.
- 106 J. Russo and H. Tanaka, *Nat. Commun.*, 2014, **5**, year.
- 107 H. B. Callen, *Thermodynamics and an Introduction to Thermostatistics*, John Wiley & Sons, 2006.
- 108 H. E. Stanley, S. Buldyrev, M. Canpolat, O. Mishima, M. Sadr-Lahijany, A. Scala and F. Starr, *Phys. Chem. Chem. Phys.*, 2000, **2**, 1551–1558.
- 109 D. Paschek, *Phys. Rev. Lett.*, 2005, **94**, 217802.
- 110 A. Nilsson and L. Pettersson, *Chem. Phys.*, 2011, **389**, 1–34.